



RESEARCH LETTER

10.1002/2017GL075857

Key Points:

- Sporadic K layers with a density exceeding $1,000 \text{ cm}^{-3}$ observed near Beijing, more than 4 times higher than previously reported
- The K/Na ratio is enhanced to 0.2, compared with the chondritic ratio of around 0.06
- Explained by differences in the ion-molecule chemistry of K^+ and Na^+ ions during the tidally driven descent of a sporadic E layer

Supporting Information:

- Supporting Information S1

Correspondence to:

J. M. C. Plane,
j.m.c.plane@leeds.ac.uk

Citation:

Jiao, J., Yang, G., Wang, J., Feng, W., & Plane, J. M. C. (2017). Observations of dramatic enhancements to the mesospheric K layer. *Geophysical Research Letters*, 44, 12,536–12,542. <https://doi.org/10.1002/2017GL075857>

Received 27 SEP 2017

Accepted 7 DEC 2017

Accepted article online 13 DEC 2017

Published online 26 DEC 2017

Observations of Dramatic Enhancements to the Mesospheric K Layer

J. Jiao^{1,2} , G. Yang¹ , J. Wang¹, W. Feng^{2,3} , and J. M. C. Plane² 

¹State Key Laboratory of Space Weather, National Space Science Center, Chinese Academy of Sciences, Beijing, China, ²School of Chemistry, University of Leeds, Leeds, UK, ³National Centre for Atmospheric Science, School of Earth and Environment, University of Leeds, Leeds, UK

Abstract Highly concentrated layers of atomic K have been observed in the mesosphere above Yanqing near Beijing (40°N, 116°E). The K density in these narrow layers exceeds $1,100 \text{ cm}^{-3}$ (at least 4 times higher than reported elsewhere), and the K/Na ratio is superchondritic by a factor of 3–4. A model with detailed metal ion chemistry, supported by ancillary measurements from a nearby ionosonde and meteor radar, is used to show that these sporadic K layers can be produced from a strong sporadic E layer (critical frequency $> 11 \text{ MHz}$) that descends from above 100 km at a velocity of $1\text{--}2 \text{ km h}^{-1}$. This allows most of the Na^+ ions to be neutralized before the remaining ions are dumped around 90 km, where the higher pressures and colder temperatures facilitate the formation of $\text{K}^+\cdot\text{N}_2$ and $\text{K}^+\cdot\text{CO}_2$ cluster ions. These cluster ions then undergo dissociative recombination with electrons to form K.

Plain Language Summary The source of metallic atoms in the Earth's upper atmosphere is the ablation of cosmic dust particles. These metals exist in layers between 80 and 105 km. Under most circumstances, the abundance of K is about 1/15 that of Na, the same ratio as in cosmic dust. However, in this study near Beijing, thin layers of K with a concentration more than 4 times that previously reported were observed, accompanied by a dramatic increase in the K/Na ratio to 1/5. These observations are explained by a wind shear above 100 km producing a highly concentrated layer of metal ions and electrons, which then descends over more than 5 h to around 90 km. K ions only neutralize at relatively high pressures and low temperatures, and this occurs around 90 km where a concentrated layer of neutral K atoms then forms. Because Na ions are mostly neutralized at higher altitudes, a large increase in the K/Na in the layer results.

1. Introduction

Meteoritic ablation is the source of the layers of Na and K atoms that occur globally at an altitude between 80 and 105 km. The layers have been observed from geographically widespread locations using the ground-based resonance lidar technique and also from space by satellite-borne spectrometric observations of solar-pumped resonance fluorescence (Plane et al., 2015). These observations have also been modeled successfully in a whole atmosphere chemistry-climate model (Dawkins et al., 2015; Marsh et al., 2013). Although the K/Na ratio is generally close to the value of 0.06 found in carbonaceous chondrites (Asplund et al., 2009), at high latitudes, the ratio varies from 0.1 in summer to 0.02 in winter (Dawkins et al., 2015).

Sporadic Na and K layers (termed Na_s and K_s) are thin layers (typically $< 2 \text{ km}$ vertical extent) of these metal atoms, develop peak densities at least 3 times larger than the typical metal background layer, and exhibit a duration of between only a few minutes and several hours (Clemesha, 1995). Following the observation of a close spatial and temporal correlation between sporadic E layers (termed E_s) and sporadic neutral metal layers, the most widely accepted mechanism to explain Na_s layers is the neutralization of Na^+ ions in a descending E_s layer (Cox & Plane, 1998; von Zahn & Hansen, 1988). This theory has also been supported by laboratory studies of the relevant ion-molecule chemistry (Cox & Plane, 1998) and modeling (Collins et al., 2002; Heinselman, 2000). A comparison of satellite measurements of Na_s and K_s occurrence probabilities reveals significant geographic and seasonal differences (Dawkins et al., 2015; Fan et al., 2007). These differences may be caused by differences in the chemistry of these two alkali ions, which also largely account for the different seasonal behaviors of the background Na and K layers (Plane et al., 2014).

In this paper we will report observations of extremely high concentrations of atomic K over Yanqing near Beijing (40°N, 116°E), more than a factor of 4 times higher than the previously published highest density ($\sim 400 \text{ cm}^{-3}$) of which we are aware. The reported maximum K concentrations at various locations are low

latitudes, 100 cm^{-3} at Arecibo (18°N) (Friedman et al., 2013) and 71 cm^{-3} at Tenerife (28°N) (Fricke-Begemann et al., 2002); midlatitudes, 360 cm^{-3} at K hlungsborn (54°N) (Eska et al., 1998) and 300 cm^{-3} at Haute Provence (40°N) (Megie et al., 1978); and high latitudes, 90 cm^{-3} at Spitsbergen (78°N) (H ffner & L bken, 2007). The highest density K_s layer observed by the Odin satellite was 230 cm^{-3} (Dawkins et al., 2015). von Zahn et al. (1999) reported a K concentration of 376 cm^{-3} in a thin layer, but this was a freshly ablated meteor trail. In the present study we will describe simultaneous K and Na measurements on two nights—one with an extreme K_s layer and abnormally high K/Na ratio, the other a typical background night as a reference. The mechanism for the K_s layer formation will then be explored using a model of a descending E_s layer with detailed ion-molecule chemistry, supported by ancillary measurements of wind and electron density.

2. Data and Methods

The Yanqing Na-K lidar is a two-channel system that can be used to observe Na atoms (589 nm) and K atoms (770 nm) simultaneously. The temporal and spatial resolutions of the lidar are 2.8 min and 96 m, respectively, with a beam divergence of 0.5 mrad (Jiao et al., 2015).

The absolute K density measured by the lidar was corrected for saturation effects, using the relation (Chu & Pappen, 2005; Megie et al., 1978):

$$\frac{N^{\text{sat}}(z)}{N(z)} = \frac{1}{1 + \frac{\tau}{t_{\text{sat}}}} \left\{ 1 - \frac{\tau}{t_L} \frac{\frac{\tau}{t_{\text{sat}}}}{1 + \frac{\tau}{t_{\text{sat}}}} \left[\exp\left(-\frac{t_L}{\tau} \left(1 + \frac{\tau}{t_{\text{sat}}}\right)\right) - 1 \right] \right\}$$

where $N^{\text{sat}}(z)$ is the photon counts received at height z ; $N(z)$ would be the photon counts from height z in the absence of saturation; τ is the lifetime of the $4^2P_{1/2}$ excited state of the K D_1 line; t_L is the pulse width of the laser; and $t_{\text{sat}} = \frac{\pi t_L z^2 \theta_L^2}{8\sigma_{\text{eff}} N_L T_r}$ is the ‘‘saturation time,’’ where θ_L is the beam divergence of the laser, N_L is the total photon number emitted in each laser pulse, and T_r is the one-way atmospheric transmission. For the current K lidar system, $N_L = 1.74 \times 10^{17}$ counts; assuming atmospheric transmission $T_r = 0.7$ (Megie et al., 1978) at 770 nm and $z = 90$ km (i.e., around the layer peak), the saturation time t_{sat} is 116 ns. Thus, the ratio $\frac{N^{\text{sat}}(z)}{N(z)} = 96.3\%$, and this was used to correct the measured counts, before smoothing using a Hamming function with a 5 min, 96 m window. The photon counts in the altitude range 170–190 km were used as background noise and deducted in the density calculation. The corresponding saturation ratio for Na is 97.8%. We assign a 10% uncertainty to these saturation corrections. There is an additional 5% uncertainty in the Na signal that arises from the nonlinear response of the photomultiplier at the higher photon count rate; this is corrected using the method of Guan et al. (2013). The photon noise-induced uncertainties are $\sim 1\%$ and $\leq 10\%$ for Na and K, respectively. The effective resonance scattering cross section for the Na D2 line is $\sim 5.2 \times 10^{-12} \text{ cm}^2$, and for the K D1 line is $\sim 5.0 \times 10^{-12} \text{ cm}^2$, calculated using temperatures from the NRLMSIS-00 model (Picone et al., 2002). The estimated uncertainty of these cross sections is around 20%. The reference air density at 30 km altitude was taken as the nighttime average from the NRLMSIS-00 model for the particular night of observation, at the latitude and longitude of the lidar. The uncertainty in the reference air density is estimated to be around 20%. Propagating all these sources of error yields uncertainties in the Na and K atom densities at the layer peaks of up to 30%.

The E_s layer electron density was determined using the Beijing ionosonde, which has a 1 h temporal resolution (Hu et al., 2014). Horizontal wind data were provided from the Beijing meteor radar, with a 1 h temporal and 2 km vertical resolution (Jiang et al., 2012). The ionosonde and meteor radar are located at Peking University (Changping district, Beijing) (40.3°N , 116.3°E), which is 40 km from the Yanqing lidar. The Changping ionosonde field-of-view is 60° , corresponding to a horizontal distance of ~ 58 km for an E_s height of 100 km, so that the Yanqing lidar is within range.

3. Results and Discussion

The seasonal K density measured with the Yanqing lidar exhibits a semiannual variation with a maximum of 110 cm^{-3} in winter and a second maximum of 85 cm^{-3} in summer (Wang et al., 2017), in good accord with the zonal average measured by satellite (Dawkins et al., 2015). However, K_s layers are observed at this location with much higher densities than previously reported elsewhere: out of a total of 809 h of observation, K

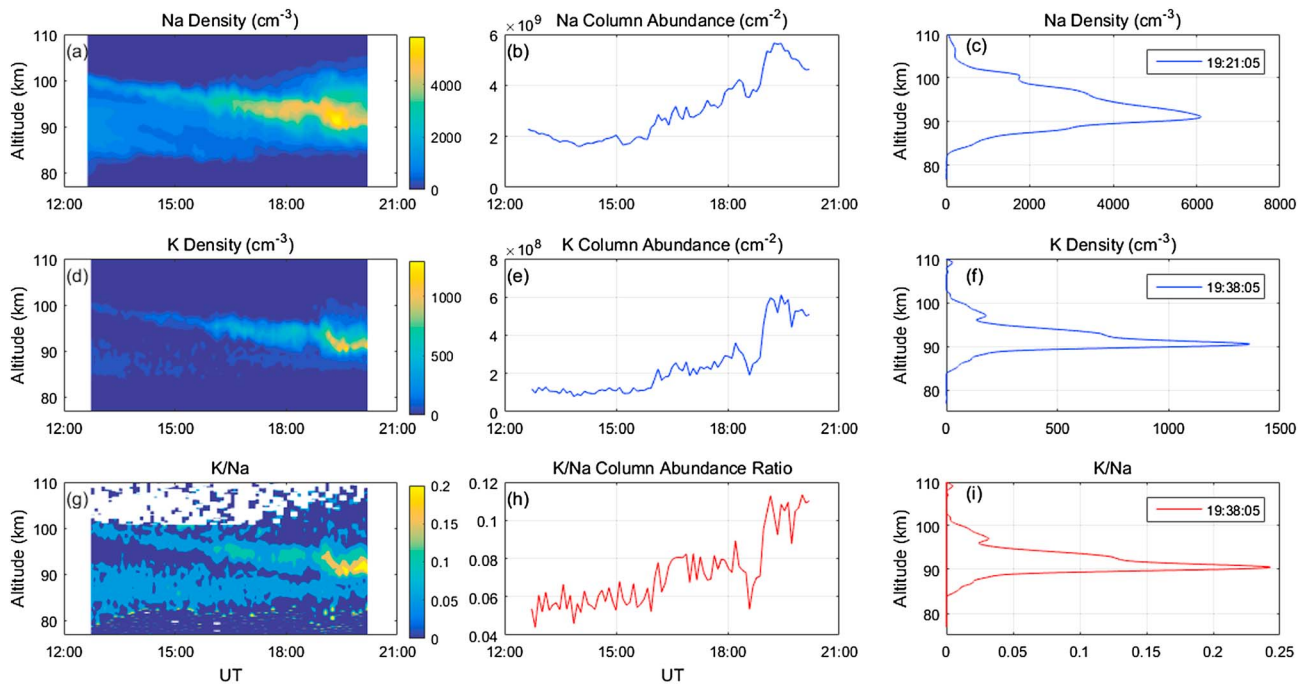


Figure 1. Na and K densities on 23 July 2013 at Yanqing (local time = UT + 8 h): (a) Na density versus height and time; (b) Na column abundance versus time; (c) vertical profile of Na density at the time of peak Na concentration (19:21 UT); (d) K density versus height and time; (e) K column abundance versus time; (f) vertical profile of K density at the time of peak of the K concentration (19:38 UT); (g) K/Na density ratio as a function of height and time; (h) K/Na column abundance ratio versus time; (i) vertical profile of the K/Na ratio at 19:38 UT.

densities above 500 cm^{-3} are observed 1.7% of the time, and densities above $1,000 \text{ cm}^{-3}$ occur with a $\sim 0.3\%$ probability.

Figure 1 illustrates an example of an extreme K_s layer that was observed on the night of 23 July 2013. The time series of Na and K density profiles (Figures 1a and 1d, respectively) show the Na_s and K_s layers descending at a speed of $1\text{--}2 \text{ km h}^{-1}$ over about 7 h, essentially throughout the night. This is good evidence for a layer with large-scale horizontal homogeneity and justifies the use of the 1-D model described below. The time series of Na and K column abundances (Figures 1b and 1e, respectively) show that these grew in a similar fashion over the course of the night. However, the Na/K column abundance ratio (Figure 1h) reveals that the K column abundance grew more quickly, particularly after 18:30 UT. This is also clear from inspection of the K density profile time series (Figure 1d) and the K/Na density ratio profile time series (Figure 1g). In fact, the K column abundance exceeds $5 \times 10^8 \text{ cm}^{-2}$ at the end of the night, which is an order of magnitude higher than the 40°N zonal average in July (Dawkins et al., 2015). Figure 1c shows the maximum density Na profile, which occurred 17 min earlier than the maximum K density (Figure 1f). Note also that the peak K layer is much narrower than the peak Na layer and occurs 1–2 km lower. Strikingly, the maximum K density is $1,363 \text{ cm}^{-3}$. The maximum ratio K/Na ratio profile (Figure 1i) shows that the peak value of the ratio is 0.23, that is, ~ 4 times larger than the background ratio.

An interesting contrast to the conditions of Figure 1 is shown in Figure 2, where the Na and K layers were observed by the Yanqing lidar over 13 h during the night of 17 December 2013. Both the Na and K layers are broader compared to the summertime layers shown in Figure 1, especially on their bottom sides, and have lower peak heights (Figures 2a and 2d). The column density time series plots (Figures 2b and 2e) show that the Na and K column densities increased significantly during this night. However, in contrast to Figure 1, the peak K/Na density ratio (Figure 2g) remained essentially constant around 0.06 at 85 km (Figure 2h), and the column density ratio (Figure 2h) had a near-constant value of ~ 0.04 . These values are in accord with previous ground-based and satellite observations (Dawkins et al., 2015; Plane, 2003) and the chondritic K/Na ratio of 0.06 (Asplund et al., 2009). Note that the layers also peaked at very different times: the Na layer at 15:35 UT with a peak density of $4,800 \text{ cm}^{-3}$ at 88 km (Figure 2c) and the K layer at 21:38:05 UT with a peak

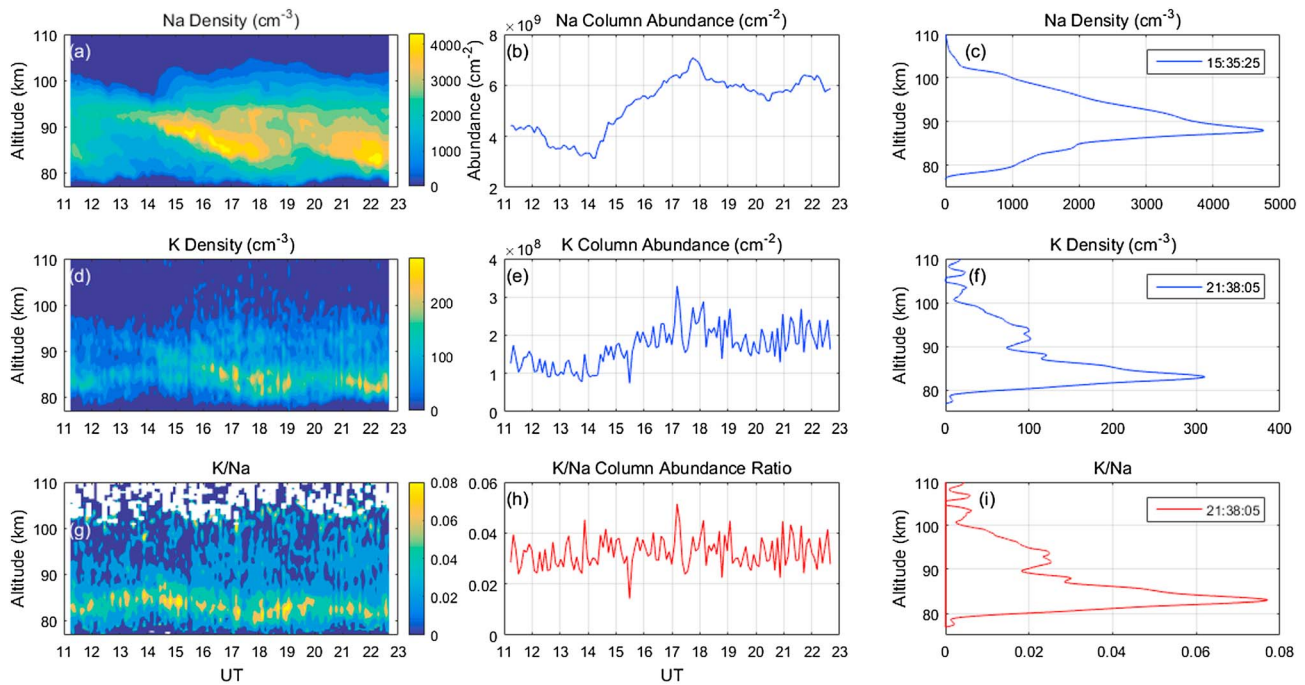


Figure 2. Na and K densities on 17 December 2013: (a) Na density versus height and time; (b) Na column abundance versus time; (c) vertical profile of Na density at the time of peak Na concentration (15:35 UT); (d) K density versus height and time; (e) K column abundance versus time; (f) vertical profile of K density at the time of peak of the K concentration (21:38 UT); (g) K/Na density ratio as a function of height and time; (h) K/Na column abundance ratio versus time; (i) vertical profile of the K/Na ratio at 21:38 UT.

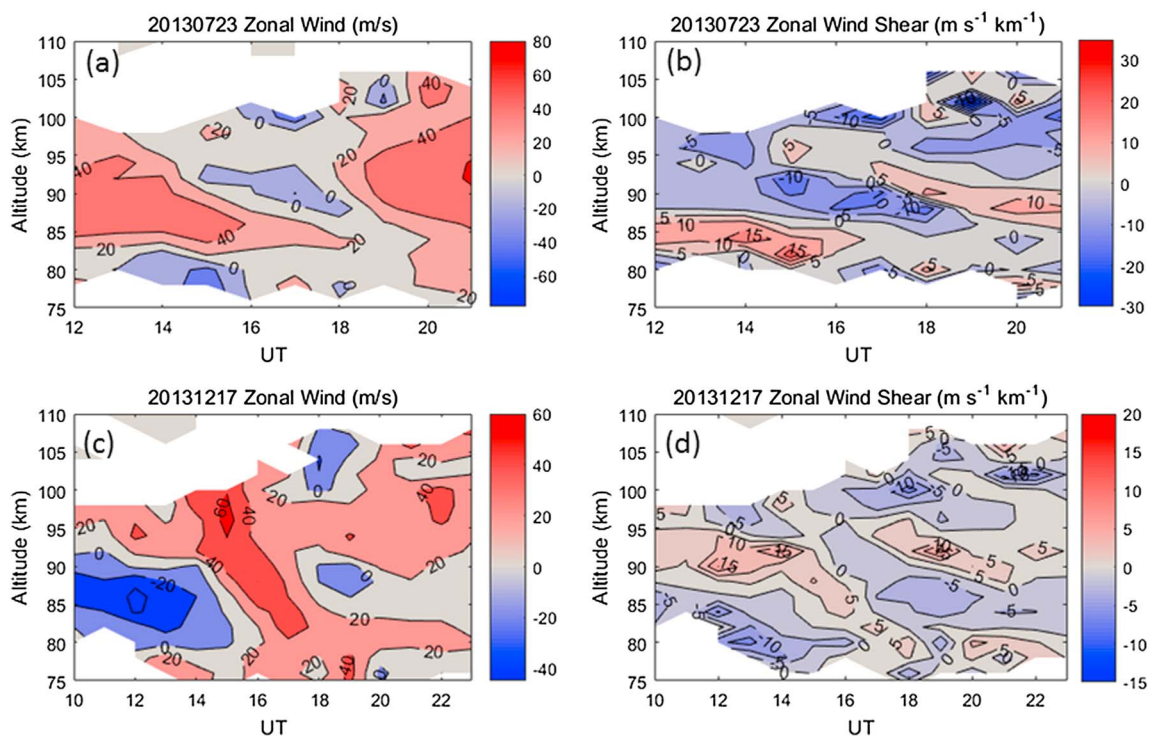


Figure 3. (a) Zonal wind on 23 July 2013; (b) zonal wind shear on 23 July 2013; (c) zonal wind on 17 December 2013; (d) zonal wind shear on 17 December 2013.

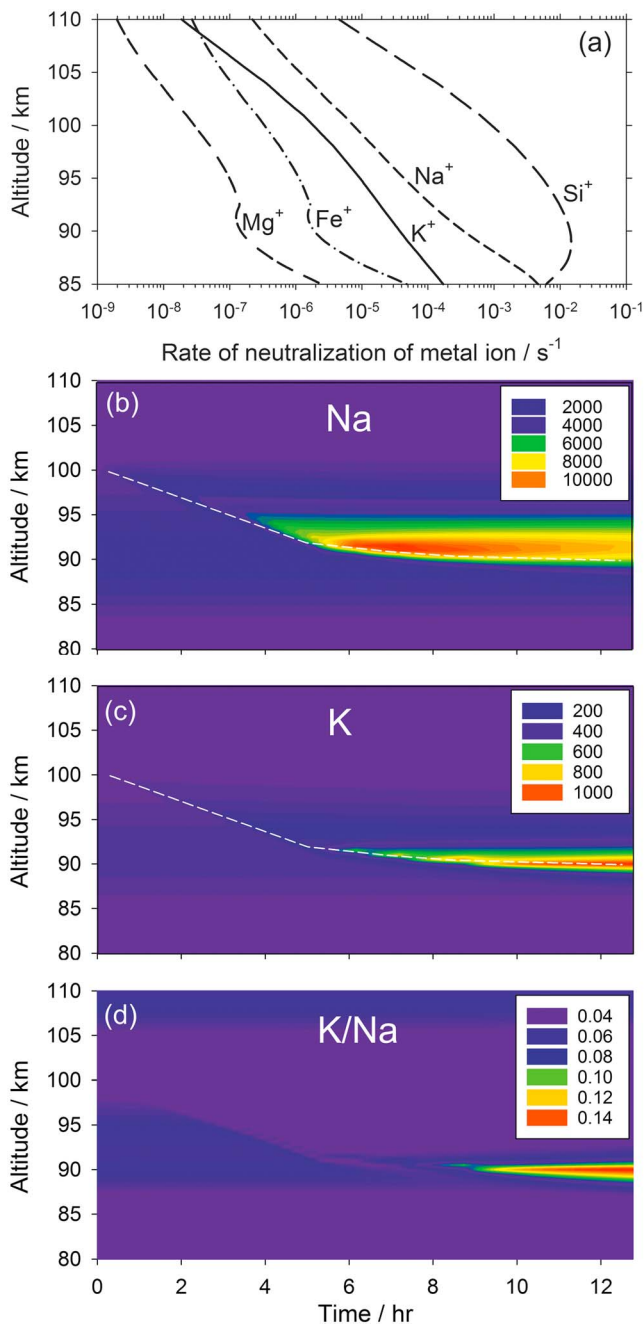


Figure 4. 1-D model simulation: (a) neutralization rates of Na^+ , K^+ , Fe^+ , Mg^+ , and Si^+ in the MLT for a background electron density. (b) Na density as a function of time and height, produced from Na^+ in a descending sporadic E layer shown by the dashed white line; (c) same as in Figure 4b but for K; (d) the $[\text{K}]/[\text{Na}]$ ratio versus time.

Tables S3 and S4, respectively), the resulting FeO^+ and MgO^+ ions are much more likely to be reduced back to Fe^+ and Mg^+ by atomic O (reaction 4 in Tables S3 and S4, respectively), rather than undergoing dissociative recombination with electrons (reaction 8 in Table S3 and reaction 9 in Table S4, respectively). In fact, Fe^+ and Mg^+ are neutralized more slowly than Na^+ and K^+ between 90 and 105 km. This means that during the descent of an E_s layer down to 90 km, the electron density can remain relatively high, so that the neutralization rates of Na^+ and K^+ are effectively decoupled from the major metallic ions in the E_s layer. Second, K^+ is neutralized 5–10 times more slowly than Na^+ . This is because K^+ is a larger ion than Na^+ , and the resulting weaker

density of $\sim 310 \text{ cm}^{-3}$ at 84 km (Figure 2f). That is, the K layer peaked ~ 6 h later and 4 km lower than the Na layer.

The important difference between the two example cases is that the Na_s and K_s layers in Figure 1 started descending from around 100 km (Figures 1a and 1d), whereas in Figure 2, there is no evidence of a descending layer. The Na_s and K_s layers are therefore very likely to have been produced from an E_s layer. Indeed, there is an usually high occurrence frequency of E_s in the East Asia region during summer (Wu et al., 2005), which is consistent with satellite observations of a relatively high occurrence of K_s layers (Figure 10 in Dawkins et al., 2015). E_s layers form at wind shears and can then undergo vertical transport by atmospheric tides (Mathews, 1998). The classical mechanism for E_s formation at mid-latitudes requires a westward wind above an eastward wind, with the resulting Lorentz force concentrating metallic ions at the null point of wind shear (Chimonas & Axford, 1968). The E_s layer is largely composed of metallic ions because they are atomic and thus do not undergo dissociative recombination with electrons, unlike ambient NO^+ and O_2^+ ions.

Figure 3a shows the zonal wind profile time series measured with the Changping meteor radar on 23 July 2013 (i.e., corresponding to Figure 1). From 14:30 to 18:30 UT, the null point in the wind shear descended with a velocity of 1–2 km h^{-1} , with the westward wind above and eastward wind below, therefore favoring the convergence of metallic ions. The maximum negative zonal wind shears (Figure 3b) are $-15.0 \text{ ms}^{-1} \text{ km}^{-1}$ at 92 km at 15:00 UT, $-14.1 \text{ ms}^{-1} \text{ km}^{-1}$ at 90 km at 17:00 UT, and $-13.6 \text{ ms}^{-1} \text{ km}^{-1}$ at 88 km at 18:00 UT. This rate of descent corresponds closely to the descent of the K_s and Na_s layers (Figures 1a and 1d). In contrast, on 17 December 2013, the wind shear was reversed (eastward wind above westward wind), and the negative wind shear values were much smaller (Figures 3c and 3d).

We now employ a 1-D model (Bones et al., 2016; Cox & Plane, 1998) to investigate how Na and K would be released from a descending E_s layer. The ion-molecule chemistry of both alkali metals along with the major meteoric species Fe, Mg, and Si were included in the model. The Tables S1–S5 in the supporting information list the relevant reactions and rate coefficients for Na^+ , K^+ , Fe^+ , Mg^+ , and Si^+ , respectively (Plane et al., 2015, 2016; Rollason & Plane, 1998), as well as analytic steady state expressions (Plane, 2004) for calculating the rate of neutralization of each metal ion as a function of height. These first-order rates are plotted in Figure 4a, for the case of a background electron density profile (Bilitza & Reinisch, 2008). There are two points to note. First, Si^+ is neutralized more rapidly than the other atomic ions because the dissociative charge transfer reaction $\text{Si}^+ + \text{O}_3 \rightarrow \text{SiO} + \text{O}_2^+$ (reaction 4 in Table S5) causes the direct neutralization of Si^+ . In contrast, while the other major ions Fe^+ and Mg^+ also react with O_3 (reaction 3 in

electrostatic forces cause cluster formation through pressure-dependent association reactions with N_2 , O_2 , and CO_2 to be slower (Tables S1 and S2); furthermore, the resulting clusters dissociate more rapidly (e.g., reaction 4 in Table S2) unless the temperature is relatively low (Plane et al., 2014). This means that K^+ will tend to be neutralized later than Na^+ as the descending E_s layer encounters higher pressures and lower temperatures.

The E_s layer was initialized with relative metallic ion ratios of $K^+ : Na^+ : Mg^+ : Fe^+ : Si^+ = 1 : 10 : 35 : 67 : 80$, based on measurements by rocket-borne mass spectrometry above 95 km (Kopp, 1997). Background atmospheric densities of O_3 , O , total density, and temperature were taken from the MESOMOD model (Murray & Plane, 2005). In accord with the observed sporadic layers in Figure 1, the model E_s layer was set to descend from 100 km at a velocity of 1.7 km h^{-1} , taking 5.9 h to reach 90 km (the track of the E_s is depicted with a dashed white line in Figures 4b and 4c). In order to generate the observed K density of $\sim 1,100 \text{ cm}^{-3}$ on 23 July 2013 (Figure 1c), the E_s layer was initialized with a peak electron density of $1.7 \times 10^6 \text{ cm}^{-3}$ and a full width at half maximum of 1.5 km. This electron density would correspond to an ionosonde critical frequency $f_c = 11.6 \text{ MHz}$, which is slightly lower than the value of 12.9 MHz measured at 13:00 UT on that day with the Changping ionosonde, located 40 km from the lidar. The modeled electron density in the E_s layer decreased to $8.0 \times 10^4 \text{ cm}^{-3}$ —that is, by a factor of ~ 20 —by the end of the model run (12.7 h after the descent commenced). Note that the sporadic layer is assumed to have a large horizontal homogeneous extent so that advection does not play a role while the layer is descending, which is a necessary condition for the 1-D model to be valid.

The modeled release of Na and K from the descending E_s is shown in Figures 4b and 4c, and the K/Na ratio in Figure 4d. As expected, Na is released earlier and higher up than K, which is only released to any significant extent once the descent of the E_s layer ceases around 90 km. The resulting sporadic K layer density exceeds $1,100 \text{ cm}^{-3}$, and the K/Na ratio approaches 0.2, as observed (Figure 1). Although the density in the modeled sporadic Na layer (Figure 4b) is roughly twice that observed, given the simplifications involved in a 1-D representation, we consider that the overall agreement is strong enough to support this explanation for the unusually concentrated K layer.

A final point to note is that such high K_s densities were not observed from the Odin satellite (Dawkins et al., 2015). However, these spaceborne measurements used spectroscopic observations of K emission in the day-glow and thus at the local time of the satellite (~ 0600 and 1800 h), in contrast to the very concentrated K_s layers reported in this study that tend to appear around local midnight.

4. Conclusions

In this study we report observations of narrow layers of atomic K with densities at least 4 times higher than previously published. The K/Na ratio in these layers is also ~ 4 times larger than chondritic. The conditions that appear to be required to generate the K_s layers are (1) a strong sporadic E layer that starts descending from above 100 km; (2) a rate of descent ($1\text{--}2 \text{ km h}^{-1}$) that allows Na^+ ions to be mostly neutralized above the altitude where the remaining ions are dumped; and (3) a dump altitude around 90 km, where the pressure is high enough and the temperature cold enough to facilitate the formation of $K^+ \cdot N_2$ and $K^+ \cdot CO_2$ ions, which can then undergo dissociative recombination with electrons to form K. These conditions were met on the night of 23 July 2013 (Figure 1), but not on 17 December 2013 (Figure 2), where, although there was significant variability in the Na and K layers, the horizontal wind structure did not facilitate formation and descent of a sporadic E layer, so that the K/Na ratio remained essentially chondritic.

References

- Asplund, M., Grevesse, N., Sauval, A. J., & Scott, P. (2009). The chemical composition of the Sun. In R. Blandford, J. Kormendy, & E. van Dishoeck (Eds.), *Annual review astronomy and astrophysics* (pp. 481–522). Palo Alto: Annual Reviews.
- Billitza, D., & Reinisch, B. (2008). International reference ionosphere 2007: Improvements and new parameters. *Advances in Space Research*, 42(4), 599–609. <https://doi.org/10.1016/j.asr.2007.07.048>
- Bones, D. L., Gerding, M., Hoffner, J., Martin, J. C. G., & Plane, J. M. C. (2016). A study of the dissociative recombination of CaO^+ with electrons: Implications for Ca chemistry in the upper atmosphere. *Geophysical Research Letters*, 43, 12,333–12,339. <https://doi.org/10.1002/2016GL071755>
- Chimonas, G., & Axford, W. I. (1968). Vertical movement of temperate zone sporadic E layers. *Journal of Geophysical Research*, 73(1), 111–117. <https://doi.org/10.1029/JA073i001p00111>
- Chu, X., & Papen, G. C. (2005). Resonance fluorescence lidar for measurements of the middle and upper atmosphere. In T. Fujii & T. Fukuchi (Eds.), *Laser remote sensing* (pp. 179–432). Boca Raton, FL: CRC Press. <https://doi.org/10.1201/9781420030754.ch5>

Acknowledgments

This work was supported by the European Research Council (project 291332-CODITA), the Natural Science Foundation of China (41474130, 41604130 and 41264006), the Chinese Meridian Project, the NSSC research fund for key development directions, and the Specialized Research Fund for State Key Laboratories of China. The meteor radar data were obtained from World Data Centre for Geophysics, Beijing (<http://wdc.geophys.ac.cn/dbView.asp>), and we thank Lianhuan Hu for providing the ionosonde data. The lidar, meteor radar, and ionosonde data used in the study and the model output have been archived at the Leeds University PETAL (PetaByte Environmental Tape Archive and Library, <http://www.see.leeds.ac.uk/business-and-consultation/facilities/petabyte-environmental-tape-archive-and-library-petal/>).

- Clemesha, B. R. (1995). Sporadic neutral metal layers in the mesosphere and lower thermosphere. *Journal of Atmospheric and Solar - Terrestrial Physics*, 57(7), 725–736. [https://doi.org/10.1016/0021-9169\(94\)00049-T](https://doi.org/10.1016/0021-9169(94)00049-T)
- Collins, S. C., Plane, J. M. C., Kelley, M. C., Wright, T. G., Soldán, P., Kane, T. J., ... Tepley, C. A. (2002). A study of the role of ion-molecule chemistry in the formation of sporadic sodium layers. *Journal of Atmospheric and Solar - Terrestrial Physics*, 64(7), 845–860. [https://doi.org/10.1016/S1364-6826\(02\)00129-3](https://doi.org/10.1016/S1364-6826(02)00129-3)
- Cox, R. M., & Plane, J. M. C. (1998). An ion-molecule mechanism for the formation of neutral sporadic Na layers. *Journal of Geophysical Research*, 103(D6), 6349–6359. <https://doi.org/10.1029/97JD03376>
- Dawkins, E. C. M., Plane, J. M. C., Chipperfield, M. P., & Feng, W. (2015). The near-global mesospheric potassium layer: Observations and modeling. *Journal of Geophysical Research: Atmospheres*, 120, 7975–7987. <https://doi.org/10.1002/2015JD023212>
- Eska, V., Hoffner, J., & von Zahn, U. (1998). Upper atmosphere potassium layer and its seasonal variations at 54 degrees N. *Journal of Geophysical Research*, 103(A12), 29,207–29,214. <https://doi.org/10.1029/98JA02481>
- Fan, Z. Y., Plane, J. M. C., & Gumbel, J. (2007). On the global distribution of sporadic sodium layers. *Geophysical Research Letters*, 34, L15808. <https://doi.org/10.1029/2007GL030542>
- Fricke-Begemann, C., Höffner, J., & von Zahn, U. (2002). The potassium density and temperature structure in the mesopause region (80–105 km) at a low latitude (28°N). *Geophysical Research Letters*, 29(22), 2067. <https://doi.org/10.1029/2002GL015578>
- Friedman, J. S., Chu, X., Brum, C. G. M., & Lu, X. (2013). Observation of a thermospheric descending layer of neutral K over Arecibo. *Journal of Atmospheric and Solar - Terrestrial Physics*, 104, 253–259. <https://doi.org/10.1016/j.jastp.2013.03.002>
- Guan, S., Yang, G., Chang, Q., Cheng, X., Yang, Y., Gong, S., & Wang, J. (2013). New methods of data calibration for high power-aperture lidar. *Optics Express*, 21(6), 7768–7785. <https://doi.org/10.1364/OE.21.007768>
- Heinselmann, C. J. (2000). Auroral effects on the gas phase chemistry of meteoric sodium. *Journal of Geophysical Research*, 105(D10), 12,181–12,192. <https://doi.org/10.1029/2000JD900085>
- Höffner, J., & Lübken, F. J. (2007). Potassium lidar temperatures and densities in the mesopause region at Spitsbergen (78°N). *Journal of Geophysical Research*, 112, D20114. <https://doi.org/10.1029/2007JD008612>
- Hu, L., Ning, B., Liu, L., Zhao, B., Li, G., Wu, B., ... Wu, Z. (2014). Validation of COSMIC ionospheric peak parameters by the measurements of an ionosonde chain in China. *Annales de Geophysique*, 32(10), 1311–1319. <https://doi.org/10.5194/angeo-32-1311-2014>
- Jiang, G., Xu, J., Yuan, W., Ning, B., Wan, W., & Hu, L. (2012). A comparison of mesospheric winds measured by FPI and meteor radar located at 40N. *SCIENCE CHINA Technological Sciences*, 55(5), 1245–1250. <https://doi.org/10.1007/s11431-012-4773-1>
- Jiao, J., Yang, G., Wang, J., Cheng, X., Li, F., Yang, Y., ... Gong, S. (2015). First report of sporadic K layers and comparison with sporadic Na layers at Beijing, China (40.6 degrees N, 116.2 degrees E). *Journal of Geophysical Research: Space Physics*, 120, 5214–5225. <https://doi.org/10.1002/2014JA020955>
- Kopp, E. (1997). On the abundance of metal ions in the lower ionosphere. *Journal of Geophysical Research*, 102(A5), 9667–9674. <https://doi.org/10.1029/97JA00384>
- Marsh, D. R., Janches, D., Feng, W., & Plane, J. M. C. (2013). A global model of meteoric sodium. *Journal of Geophysical Research: Atmospheres*, 118, 11,442–11,452. <https://doi.org/10.1002/jgrd.50870>
- Mathews, J. D. (1998). Sporadic E: Current views and recent progress. *Journal of Atmospheric and Solar - Terrestrial Physics*, 60(4), 413–435. [https://doi.org/10.1016/S1364-6826\(97\)00043-6](https://doi.org/10.1016/S1364-6826(97)00043-6)
- Megie, G., Bos, F., Blamont, J. E., & Chanin, M. L. (1978). Simultaneous nighttime lidar measurements of atmospheric sodium and potassium. *Planetary and Space Science*, 26(1), 27–35. [https://doi.org/10.1016/0032-0633\(78\)90034-x](https://doi.org/10.1016/0032-0633(78)90034-x)
- Murray, B. J., & Plane, J. M. C. (2005). Modelling the impact of noctilucent cloud formation on atomic oxygen and other minor constituents of the summer mesosphere. *Atmospheric Chemistry and Physics*, 5(4), 1027–1038. <https://doi.org/10.5194/acp-5-1027-2005>
- Picone, J. M., Hedin, A. E., Drob, D. P., & Aikin, A. C. (2002). NRLMSISE-00 empirical model of the atmosphere: Statistical comparisons and scientific issues. *Journal of Geophysical Research*, 107(A12), 1468. <https://doi.org/10.1029/2002JA009430>
- Plane, J. M. C. (2003). Atmospheric chemistry of meteoric metals. *Chemical Reviews*, 103(12), 4963–4984. <https://doi.org/10.1021/cr0205309>
- Plane, J. M. C. (2004). A time-resolved model of the mesospheric Na layer: Constraints on the meteor input function. *Atmospheric Chemistry and Physics*, 4(3), 627–638. <https://doi.org/10.5194/acp-4-627-2004>
- Plane, J. M. C., Feng, W., & Dawkins, E. C. M. (2015). The mesosphere and metals: Chemistry and changes. *Chemical Reviews*, 115(10), 4497–4541. <https://doi.org/10.1021/cr500501m>
- Plane, J. M. C., Feng, W., Dawkins, E., Chipperfield, M. P., Höffner, J., Janches, D., & Marsh, D. R. (2014). Resolving the strange behavior of extraterrestrial potassium in the upper atmosphere. *Geophysical Research Letters*, 41, 4753–4760. <https://doi.org/10.1002/2014GL060334>
- Plane, J. M. C., Gómez-Martín, J. C., Feng, W., & Janches, D. (2016). Silicon chemistry in the mesosphere and lower thermosphere. *Journal of Geophysical Research: Atmospheres*, 121, 3718–3728. <https://doi.org/10.1002/2015JD024691>
- Rollason, R. J., & Plane, J. M. C. (1998). A kinetic study of the reactions between Fe⁺ ions and O₃, O₂ and N₂. *Journal of the Chemical Society, Faraday Transactions*, 94(20), 3067–3075. <https://doi.org/10.1039/a805140b>
- von Zahn, U., Gerding, M., Höffner, J., McNeil, W. J., & Murad, E. (1999). Iron, calcium, and potassium atom densities in the trails of Leonids and other meteors: Strong evidence for differential ablation. *Meteoritics and Planetary Science*, 34(6), 1017–1027. <https://doi.org/10.1111/j.1945-5100.1999.tb01421.x>
- von Zahn, U., & Hansen, T. L. (1988). Sudden neutral sodium layers: A strong link to sporadic E layers. *Journal of Atmospheric and Terrestrial Physics*, 50(2), 93–104. [https://doi.org/10.1016/0021-9169\(88\)90047-5](https://doi.org/10.1016/0021-9169(88)90047-5)
- Wang, Z., Yang, G., Wang, J., Yue, C., Yang, Y., Jiao, J., ... Chi, W. (2017). Seasonal variations of meteoric potassium layer over Beijing (40.41°N, 116.01°E). *Journal of Geophysical Research: Space Physics*, 122, 2106–2118. <https://doi.org/10.1002/2016JA023216>
- Wu, D. L., Ao, C. O., Hajj, G. A., de la Torre Juarez, M., & Mannucci, A. J. (2005). Sporadic E morphology from GPS-CHAMP radio occultation. *Journal of Geophysical Research*, 110, A01306. <https://doi.org/10.1029/2004JA010701>